Appl. Phys. B 84, 197–203 (2006)
DOI: 10.1007/s00340-006-2221-2

Applied Physics B
Lasers and Optics

T. ČIŽMÁR
M. ŠILER
P. ZEMÁNEK✉

An optical nanotrap array movable over a milimetre range

Institute of Scientific Instruments, Academy of Sciences of the Czech Republic, Královopolská 147, 61264 Brno, Czech Republic

Received: 22 December 2005/Revised version: 20 March 2006
Published online: 26 April 2006 •

ABSTRACT We present the theoretical and experimental study of nondiffracting Bessel beams as a device for optical manipulation and confinement of nanoparticles. We express analytically the optical forces acting on a nanoparticle placed into a single and two counter-propagating non-paraxial nondiffracting beams created behind the axicon. Nanoparticle behavior in these configurations is predicted by computer simulations. Finally we demonstrate experimentally how standing waves created from two independent counter-propagating nondiffraction beams confines polystyrene beads of radii 100 nm, and organizes them into a one-dimensional chain 1 mm long. Phase shift in one beam causes the motion of the whole structure of the standing wave together with any confined objects over its extent.

PACS 42.25.-p; 42.50.Vk; 82.70.Dd

1 Introduction

Almost twenty years ago the concept of the so-called nondiffracting propagation of electromagnetic waves was proposed [1, 2]. These beams are formed by an interference of plane waves of wavevectors covering a conical surface. This interference is responsible for the very narrow core of these beams (linear focus), their nondiffracting propagation and the ability to reconstruct themselves after passing through a disturbing obstacle [3]. This feature is especially useful for multiple confinement of microobjects. The side effect of the interference is that the beam energy is split almost equally into several lateral rings and therefore only its fraction is available in the intense central core. The most simple nondiffracting beam is called the Bessel beam (BB) because its radial spatial profile is described by the Bessel function of the zero order. Experimentally so called pseudo-nondiffracting beams (PNDB) can be generated only. These beams do not exist in the whole unlimited space but only in a spatially limited volume. One can use an annular aperture placed at the focal plane of a lens, hologram [4] or an axicon [5] to obtain such beams. Figure 1 shows the PNDB obtained by passing a Gaussian beam through the axicon. Since the deviations of the PNDB from the ideal nondiffracting beams are not significant on the micro-scale distances considered in microobjects manipulations, the PNDB is frequently called the Bessel beam. In this paper we will follow this simplified terminology.

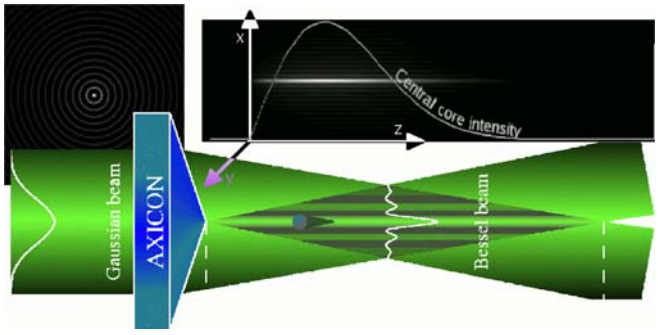

FIGURE 1 Schematic image of a nondiffracting beam generated by an axicon illuminated by a Gaussian beam. The generated beam mainly has the properties of the ideal Bessel beam – radial intensity profile is done by the zero-order Bessel function (see the radial intensity cross-section on the *top-left part*) and the axial central cross-section reveals the nondiffraction property – the same width of the central core but its intensity is influenced by illuminating Gaussian beam (*white line over*). The *bottom part* shows the generation of this so called pseudo nondiffracting beam using the axicon. This beam exists only over a distance done by the width of the illuminated part of the axicon. The inserted object only disturbs the beam significantly in a volume of a cone with the apex angle roughly determined by the angle between the generating plane wave wavevectors and the propagation axis

Because of sufficient power in the central core the axicon generated BBs are extensively used for optical guiding [6–8] and arrangement [9] of microobjects. Since the BB generation is based on the spatial and not time coherence of the light source, white-light BBs were also successfully generated [10]. Axicon has also found a number of other applications in laser machining [11], metrology [12], optical coherence tomography [13], and atomic physics [14].

Recently the properties of several BBs interfering off-axis, counter-propagating, and co-propagating were studied [15–23]. The interference of co-propagating BBs was found to be an interesting tool to generate fields with periodic axial distribution (self-imaging) [18–21]. Co-propagating BBs also create "bottle beams" – a periodic linear array of intensity minima covered by a high-intensity light field [20, 22], or an array of optical traps for high-index particles [23].

Despite the fact that a lot of applications of BBs were considered and used for optical trapping, to our knowledge

✉ Fax: +420 541 514 402, E-mail: pavlik@isibrno.cz

there is no theoretical study describing the properties of optical forces acting on nanoobjects or microobjects placed into these beams. Therefore, in this paper we focus on the theoretical description of optical trapping of nanoobjects using single BB and two counter-propagating interfering BBs, and on its experimental demonstration.

2 Ideal non-paraxial Bessel beam behind the axicon

Only a few theoretical descriptions of the vectorial nondiffracting beams were presented in the literature [24, 25] but none of them are directly applicable to the axicon illuminated by a linearly polarized beam. To simplify the theoretical description even more, let us assume that the axicon is illuminated by a linearly polarized beam that behind the axicon creates an ideal BB. Let us place the centre of the coordinate system (x, y, z) at the apex of the axicon and let us express the field behind the axicon as a spectrum of plane waves in the form [26]:

$$\boldsymbol{E}(\boldsymbol{r}) = \frac{1}{k^2}\int_{-\infty}^{\infty}\int_{-\infty}^{\infty} \boldsymbol{E}^{\mathrm{i}}_{\mathrm{PW}}(k_x, k_y)\mathrm{e}^{\mathrm{i}\boldsymbol{k}\cdot\boldsymbol{r}}\,\mathrm{d}k_x\,\mathrm{d}k_y\,, \tag{1}$$

$$\begin{aligned}\boldsymbol{B}(\boldsymbol{r}) &= \frac{1}{\mathrm{i}\omega}\nabla\times\boldsymbol{E}(\boldsymbol{r})\\ &= \frac{1}{k^2\omega}\int_{-\infty}^{\infty}\int_{-\infty}^{\infty} \boldsymbol{k}\times\boldsymbol{E}^{\mathrm{i}}_{\mathrm{PW}}(k_x, k_y)\mathrm{e}^{\mathrm{i}\boldsymbol{k}\cdot\boldsymbol{r}}\,\mathrm{d}k_x\,\mathrm{d}k_y\,,\end{aligned} \tag{2}$$

where

$$\begin{aligned}&k_x = -k\sin\alpha\cos\beta, \quad k_y = -k\sin\alpha\sin\beta\,,\\ &k_z = k\cos\alpha\,,\\ &\alpha\in\langle 0, \alpha_{\max}\rangle; \quad \alpha_{\max} < \pi/2; \quad \beta\in<0, 2\pi)\,.\end{aligned} \tag{3}$$

Using $\mathrm{d}k_x\,\mathrm{d}k_y = k^2|\sin\alpha\cos\alpha|\,\mathrm{d}\alpha\,\mathrm{d}\beta$ we get

$$\boldsymbol{E}(\boldsymbol{r}) = \int_0^{2\pi}\int_0^{\pi/2} \boldsymbol{E}^{\mathrm{i}}_{\mathrm{PW}}(\alpha, \beta)\mathrm{e}^{\mathrm{i}\boldsymbol{k}\cdot\boldsymbol{r}}|\sin\alpha\cos\alpha|\,\mathrm{d}\alpha\,\mathrm{d}\beta\,. \tag{4}$$

The BB is created as a result of the interference of plane waves if their wavevectors cover the surface of the cone. Therefore, the distribution of polar angles for this ideal BB is done by a delta function [24, 27]:

$$\boldsymbol{E}^{\mathrm{i}}_{\mathrm{PW}}(\alpha, \beta) = \boldsymbol{E}_{\mathrm{PW}}(\alpha, \beta)\frac{\delta(\alpha-\alpha_0)}{|\sin\alpha_0|\cos\alpha_0}\,. \tag{5}$$

This gives for the electric and magnetic fields behind the axicon

$$\boldsymbol{E}(\boldsymbol{r}) = \int_0^{2\pi} \boldsymbol{E}_{\mathrm{PW}}(\alpha_0, \beta)\mathrm{e}^{\mathrm{i}\boldsymbol{k}\cdot\boldsymbol{r}}\,\mathrm{d}\beta\,, \tag{6}$$

$$\boldsymbol{B}(\boldsymbol{r}) = \int_0^{2\pi} \boldsymbol{B}_{\mathrm{PW}}(\alpha_0, \beta)\mathrm{e}^{\mathrm{i}\boldsymbol{k}\cdot\boldsymbol{r}}\,\mathrm{d}\beta\,, \tag{7}$$

where α_0 is the polar angle and β is the azimuthal angle with respect to the axicon and

$$\begin{aligned}\boldsymbol{E}_{\mathrm{PW}}(\alpha_0, \beta) &\equiv E_{\mathrm{PW}x}(\alpha_0, \beta)\boldsymbol{e}_x + E_{\mathrm{PW}y}(\alpha_0, \beta)\boldsymbol{e}_y\\ &\quad + E_{\mathrm{PW}z}(\alpha_0, \beta)\boldsymbol{e}_z\\ &= E_{\mathrm{PW0}}(\alpha_0, \beta)\left\{\left[\cos\alpha_0 + \sin^2\beta(1-\cos\alpha_0)\right]\boldsymbol{e}_x\right.\\ &\quad \left. - [(1-\cos\alpha_0)\sin\beta\cos\beta]\boldsymbol{e}_y + \sin\alpha_0\cos\beta\boldsymbol{e}_z\right\},\end{aligned} \tag{8}$$

$$\begin{aligned}\boldsymbol{B}_{\mathrm{PW}}(\alpha_0, \beta) &\equiv \frac{\boldsymbol{k}}{\omega}\times\boldsymbol{E}_{\mathrm{PW}}(\alpha_0, \beta)\\ &= B_{\mathrm{PW0}}(\alpha_0, \beta)\left\{[(\cos\alpha_0 - 1)\sin\beta\cos\beta]\boldsymbol{e}_x\right.\\ &\quad \left. + \left[1 - \sin^2\beta(1-\cos\alpha_0)\right]\boldsymbol{e}_y + \sin\alpha_0\sin\beta\boldsymbol{e}_z\right\}\,,\end{aligned} \tag{9}$$

where $\boldsymbol{e}_j$ $(j = x, y, z)$ are unit vectors of the Cartesian coordinate system, $E_{\mathrm{PW}j}(\alpha_0, \beta)$ are the components of the electric field, $E_{\mathrm{PW0}}(\alpha_0, \beta)$ is the amplitude of the electric field component of the plane wave spectrum with wavevector direction described by the polar angle α_0 and azimuthal angle β. If a beam impinges on the rotationally symmetric axicon (no dependence on β), the integration in (6), (7) can be performed and we get, in a cylindrical system of coordinates (z, ϱ, φ), for a BB propagating in positive $+$ or negative $-$ direction of z axis:

$$\begin{aligned}\boldsymbol{E}(\boldsymbol{r}) &= E_{\mathrm{B0}}(\alpha_0)\mathrm{e}^{\pm\mathrm{i}k_\parallel z}\left\{[J_0(\sigma) + J_2(\sigma)P_\perp\cos(2\varphi)]\,\boldsymbol{e}_x\right.\\ &\quad \left. + J_2(\sigma)P_\perp\sin(2\varphi)\boldsymbol{e}_y \mp \mathrm{i}2J_1(\sigma)P_\parallel\cos\varphi\boldsymbol{e}_z\right\}\,,\end{aligned} \tag{10}$$

$$\begin{aligned}\boldsymbol{B}(\boldsymbol{r}) &= B_{\mathrm{B0}}(\alpha_0)\mathrm{e}^{\pm\mathrm{i}zk_\parallel}\left\{\pm J_2(\sigma)P_\perp\sin(2\varphi)\boldsymbol{e}_x\right.\\ &\quad \left. \pm [J_0(\sigma) - J_2(\sigma)P_\perp\cos(2\varphi)]\,\boldsymbol{e}_y - \mathrm{i}2J_1(\sigma)P_\parallel\sin\varphi\boldsymbol{e}_z\right\},\end{aligned} \tag{11}$$

where E_{B0} is the amplitude of the BB on the optical axis, J_j is the Bessel function of j-th order, $\boldsymbol{k}$ the wavevector, ϱ and φ are the radial coordinate and azimuthal angle in the cylindrical system of coordinates and

$$\begin{aligned}&\varrho = \sqrt{x^2+y^2}, \quad \varphi = \arctan\frac{x}{y}\,,\\ &P_\perp = \frac{1-\cos\alpha_0}{1+\cos\alpha_0}, \quad P_\parallel = \frac{\sin\alpha_0}{1+\cos\alpha_0}, \quad P_\perp = P_\parallel^2\,,\\ &\sigma = k\varrho\sin\alpha_0, \quad k_\parallel = k\cos\alpha_0, \quad k_\perp = k\sin\alpha_0\,.\end{aligned} \tag{12}$$

$$\begin{aligned}&E_{\mathrm{B0}}(\alpha_0) = \pi E_{\mathrm{PW0}}(\alpha_0)(1+\cos\alpha_0)\,,\\ &B_{\mathrm{B0}}(\alpha_0) = \frac{k}{\omega}E_{\mathrm{B0}}(\alpha_0)\,.\end{aligned} \tag{13}$$

The time-averaged Poynting vector has the form

$$\boldsymbol{S} = \frac{1}{2\mu_0}\Re\left(\boldsymbol{E}\times\boldsymbol{B}^*\right) \tag{14}$$

and substitution from (10) and (11) gives

$$S_z(\sigma) = E^2_{\mathrm{B0}}(\alpha_0)\frac{k}{2\omega\mu_0}\left[J_0^2(\sigma) - J_2^2(\sigma)P_\perp^2\right]\,, \tag{15}$$

$$S_x(\sigma) = 0, \quad S_y(\sigma) = 0\,. \tag{16}$$

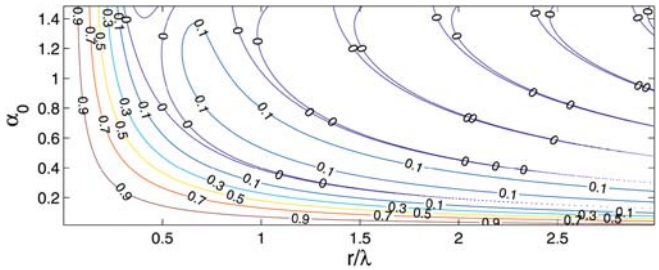

FIGURE 2 Contour plot of the normalized axial component of the Poynting vector S_z as a function of radial distance and azimuthal angle of interfering plane waves

It is seen that the Poynting vector is completely symmetrical around the propagation axis even for a non-paraxial beam, and as expected it does not depend on the longitudinal positions. With increasing angle α_0 its axial component S_z can reach negative values for certain radial positions (see Fig. 2). This indicates that in these places the energy flows opposite to the beam propagation.

Combination of several co-propagating or counter-propagating beams can be generally expressed as a sum of individual fields.

3 Optical forces acting on a nanoparticle

The optical force acting on a particle can be easily expressed for tiny (Rayleigh) particles (usually their radius fulfills $a \ll \lambda/20$). In this case the scattering is so weak that it is assumed that the particle does not modify the incident field. Therefore the ζ component of the optical force acting on such a particle can be expressed as [28]:

$$\langle F_\zeta \rangle \equiv F_\zeta = \frac{1}{2}\varepsilon_0\varepsilon_\mathrm{m}\Re\left\{\sum_{\gamma=1}^{3}\alpha E_\gamma \nabla_\zeta E_\gamma^*\right\}, \tag{17}$$

where $\nabla_\zeta \equiv \dfrac{\partial}{\partial r_\zeta}$,

ε_0 is the permittivity of vacuum, $\varepsilon_\mathrm{m} \equiv n_\mathrm{m}^2$ is the relative permittivity of the surrounding medium, $\Re$ means a real value of the expression in brackets, * is a complex conjugated value, α is a complex valued polarizability of the object given by [29] :

$$\alpha = \frac{\alpha_0}{1-\frac{2}{3}\dfrac{\mathrm{i}k^3\alpha_0}{4\pi}} \equiv \alpha' + \mathrm{i}\alpha''. \tag{18}$$

α' and α'' is the real and imaginary part of α, and α_0 is given by the by Lorentz–Lorenz relation:

$$\alpha_0 = 4\pi a^3 \frac{m^2-1}{m^2+2}, \tag{19}$$

where a is the radius of the spherical object and $m \equiv n_\mathrm{p}/n_\mathrm{m}$ is the ratio of the refractive index of the particle n_p and the surrounding medium n_m.

In the case of Rayleigh particles ($a \ll \lambda/20$) we get using (18)–(19):

$$\alpha' \simeq \alpha_0, \quad \alpha'' \simeq \frac{\alpha_0^2 k^3}{6\pi} > 0, \tag{20}$$

$$\left|\frac{\alpha''}{\alpha'}\right| = \left|\frac{2}{3}\frac{m^2-1}{m^2+2}(ka)^3\right| \ll 1. \tag{21}$$

Let us recall that $\alpha' > 0$ or $\alpha' < 0$ if $m > 1$ or $m < 1$, respectively.

Since the problem has cylindrical symmetry, we use axial, radial and azimuthal components of the force:

$$\begin{aligned}
\frac{2F_z}{\varepsilon_0\varepsilon_\mathrm{m}} &= \Re\left\{\sum_{\gamma=1}^{3}\alpha E_\gamma \frac{\partial}{\partial_z}E_\gamma^*\right\},\\
\frac{2F_\varrho}{\varepsilon_0\varepsilon_\mathrm{m}} &= \Re\left\{\sum_{\gamma=1}^{3}\alpha E_\gamma \frac{\partial}{\partial_\varrho}E_\gamma^*\right\},\\
\frac{2F_\varphi}{\varepsilon_0\varepsilon_\mathrm{m}} &= \Re\left\{\sum_{\gamma=1}^{3}\alpha E_\gamma \frac{\partial}{\varrho\,\partial_\varphi}E_\gamma^*\right\}.
\end{aligned} \tag{22}$$

3.1 *Single Bessel beam*

We focus here on a single BB propagating along the positive direction of the z axis. For brevity we will omit the argument in the Bessel functions $\sigma = k\varrho\sin\alpha_0 = k_\perp\varrho$. Putting (10) into (22) we get:

$$\begin{aligned}
\frac{2F_z}{\varepsilon_0\varepsilon_\mathrm{m}} &= \alpha'' k_\parallel E_{\mathrm{B}0}^2\left\{J_0^2 + 2J_1^2P_\parallel^2 + J_2^2P_\parallel^4\right.\\
&\quad \left. + 2\left[J_0J_2 + J_1^2\right]P_\parallel^2\cos(2\varphi)\right\},
\end{aligned} \tag{23}$$

$$\begin{aligned}
\frac{2F_\varrho}{\varepsilon_0\varepsilon_\mathrm{m}} &= \alpha' k_\perp E_{\mathrm{B}0}^2\{-J_0J_1\\
&\quad + \frac{1}{2}J_2(J_1-J_3)P_\parallel^4 + J_1(J_0-J_2)P_\parallel^2\\
&\quad + \left[\frac{3}{2}J_0J_1 - 2J_1J_2 - \frac{1}{2}J_0J_3)\right]P_\parallel^2\cos(2\varphi)\Big\},
\end{aligned} \tag{24}$$

$$\frac{2F_\varphi}{\varepsilon_0\varepsilon_\mathrm{m}} = -2\frac{\alpha'}{\varrho}E_{\mathrm{B}0}^2\sin(2\varphi)\left[J_0J_2 + J_1^2\right]P_\parallel^2. \tag{25}$$

In this type of the beam the gradient and the scattering forces are clearly distinguishable. The axial force F_z is a purely scattering force and always propels the nanoobjects in the direction of the beam propagation. On the contrary, the radial F_ϱ and azimuthal F_φ forces are purely gradient forces and objects with refractive index higher (lower) compared to the surrounding medium, are pushed to the places of higher (lower) electric field intensity. Moreover, the azimuthal force results from the non-paraxiality of the beam because it becomes negligible for wide (scalar, paraxial) beams when $P_\parallel^2 \simeq 0$:

$$\frac{2F_z}{\varepsilon_0\varepsilon_\mathrm{m}} = \alpha'' k_\parallel E_{\mathrm{B}0}^2 J_0^2, \tag{26}$$

$$\frac{2F_\varrho}{\varepsilon_0\varepsilon_\mathrm{m}} = -\alpha' k_\perp E_{\mathrm{B}0}^2 J_0J_1, \tag{27}$$

$$\frac{2F_\varphi}{\varepsilon_0\varepsilon_\mathrm{m}} = 0. \tag{28}$$

Since forces F_ϱ and F_φ are gradient forces, the potential energy of the particle in this field can be defined in the plane

perpendicular to the beam propagation for a nanoparticle fixed at a certain z position:

$$U(\varrho,\varphi) = -\frac{1}{4}\varepsilon_0\varepsilon_\mathrm{m}\alpha' \sum_{\gamma=1}^{3} E_\gamma E_\gamma^* \,. \tag{29}$$

Using (10) in (29) we get for the single BB

$$\begin{aligned} U(\varrho,\varphi) &= -\frac{1}{4}\varepsilon_0\varepsilon_\mathrm{m}\alpha' E_{\mathrm{B}0}^2 \left\{ J_0^2 + 2J_1^2 P_\parallel^2 + J_2^2 P_\parallel^4 \right. \\ &\quad \left. + 2\left[J_0 J_2 + J_1^2\right] P_\parallel^2 \cos(2\varphi) \right\} \\ &= -\frac{1}{2k_\parallel} F_z \frac{\alpha'}{\alpha''} \,. \end{aligned} \tag{30}$$

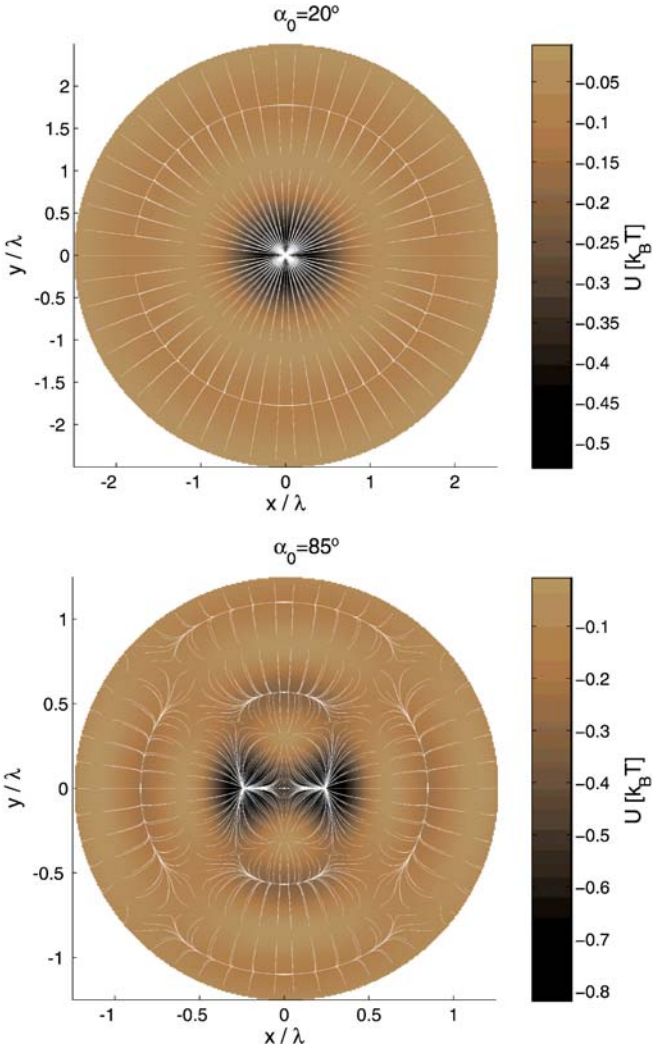

FIGURE 3 Influence of non-paraxial terms on the lateral shape of the potential (30) for small azimuthal angle $\alpha_0 = 20°$ and very big $\alpha_0 = 85°$. We assumed the wavelength in water to be $\lambda = 532/1.33$ nm, and the object was a polystyrene sphere ($n_\mathrm{p} = 1.59$) of radius $a = 10$ nm. The intensity of the electric field on the optical axis was the same as in the 1 W Gaussian beam of beam waist equal to 1 μm ($E_{\mathrm{B}0} = 1.8 \times 10^{12}$ V m^{-1}). It is seen then for the wider BB, that the non-paraxial terms are not so important and the potential minimum is in the centre of the beam. If $\alpha_0 \geq 65°$ two minima occur on the x-axis, symmetrically placed with respect to the beam centre. The *white curves* show the trajectory of the particle if it propagates from different starting positions. The colorbar shows the potential energy (in $k_\mathrm{B}T$) of the particle in the BB if the zero level is set to zero field

Figure 3 shows the examples of this potential profile for small and large α_0. For $\alpha_0 \geq 65°$ two off-axial equilibrium positions occur parallel to the polarization of the illuminating plane wave (dark spots). The depth of the potential well is less than $k_\mathrm{B}T$ for the considered particle size equal to 10 nm. This is not sufficient to radially localize the particle in the intensity maximum. Fortunately the depth of the potential well rises as a^3 for Rayleigh particles. Therefore just two to three times bigger polystyrene beads should be noticeable influenced by the BB and they should stay in the intensity maximum while they move along the z axis.

3.2 *Standing Bessel beam*

Interference of a counter-propagating BB creates a standing wave along the z axis. For simplicity let us assume that both counter-propagating beams have the same properties (except direction of propagation). Therefore, the radiation pressure coming from both beams is compensated and the resulting force is the gradient force coming from the steep intensity gradients along the z axis in the created standing wave. It was experimentally proven that this configuration can optically confine nanoparticles even in a weak Gaussian standing wave [30]. For brevity we again omit the argument $\sigma = k\varrho\sin\alpha_0$ in the Bessel functions and α_0 in $E_{\mathrm{B}0}$, and we obtain for the electric and magnetic fields:

$$\begin{aligned} \boldsymbol{E}_\mathrm{SW}(\boldsymbol{r}) &= 2E_{\mathrm{B}0}\left\{\cos(k_\parallel z)\left[J_0 + J_2 P_\perp \cos(2\varphi)\right]\boldsymbol{e}_x \right. \\ &\quad + \cos(k_\parallel z) J_2 P_\perp \sin(2\varphi)\boldsymbol{e}_y \\ &\quad \left. + 2\sin(k_\parallel z) J_1 P_\parallel \cos\varphi \boldsymbol{e}_z \right\} \,, \end{aligned} \tag{31}$$

$$\begin{aligned} \boldsymbol{B}_\mathrm{SW}(\boldsymbol{r}) &= \frac{2\mathrm{i}k}{\omega} E_{\mathrm{B}0}\left\{\sin(k_\parallel z) J_2 P_\perp \sin(2\varphi)\boldsymbol{e}_x \right. \\ &\quad + \sin(k_\parallel z)\left[J_0 - J_2 P_\perp \cos(2\varphi)\right]\boldsymbol{e}_y \\ &\quad \left. - 2\cos(k_\parallel z) J_1 P_\parallel \sin\varphi \boldsymbol{e}_z \right\} \,. \end{aligned} \tag{32}$$

Forces acting on Rayleigh particles can be expressed as:

$$\begin{aligned} \frac{2F_z^\mathrm{SW}}{\varepsilon_0\varepsilon_\mathrm{m}} &= -2\alpha' k_\parallel E_{\mathrm{B}0}^2 \sin(2k_\parallel z) \\ &\quad \times \left[J_0^2 - 2J_1^2 P_\parallel^2 + J_2^2 P_\parallel^4 + 2\cos(2\varphi)(J_0 J_2 - J_1^2) P_\parallel^2\right] \,, \end{aligned} \tag{33}$$

$$\begin{aligned} \frac{2F_\varrho^\mathrm{SW}}{\varepsilon_0\varepsilon_\mathrm{m}} &= \alpha' k_\perp E_{\mathrm{B}0}^2 \{-2J_0 J_1 \\ &\quad + J_2(J_1 - J_3) P_\parallel^4 + 2J_1(J_0 - J_2) P_\parallel^2 \\ &\quad + (3J_0 J_1 - 4J_1 J_2 - J_0 J_3)\, P_\parallel^2 \cos(2\varphi) \\ &\quad + \left[-2J_0 J_1 + J_2(J_1 - J_3) P_\parallel^4 - 2J_1(J_0 - J_2) P_\parallel^2 \right. \\ &\quad \left. - J_0\,(J_1 + J_3)\cos(2\varphi)\right] P_\parallel^2 \cos(2k_\parallel z)\} \,, \end{aligned} \tag{34}$$

$$\begin{aligned} \frac{2F_\varphi^\mathrm{SW}}{\varepsilon_0\varepsilon_\mathrm{m}} &= -4\frac{\alpha'}{\varrho} E_{\mathrm{B}0}^2 \sin(2\varphi)\left[\left(J_0 J_2 + J_1^2\right)\right. \\ &\quad \left. + \left(J_0 J_2 - J_1^2\right)\cos(2k_\parallel z)\right] P_\parallel^2 \,. \end{aligned} \tag{35}$$

In this case the system is conservative in three dimensions and therefore the potential energy for a nanoparticle in this field has the form:

$$U^\mathrm{SW}(\varrho,\varphi,z) = -\frac{1}{4}\varepsilon_0\varepsilon_\mathrm{m}\alpha' \sum_{\gamma=1}^{3} E_\gamma E_\gamma^*$$

$$= \frac{1}{2}\varepsilon_0\varepsilon_m\alpha' E_{B0}^2 \left\{2\left[\left(J_1^2 - J_0J_2\right)\cos(2k_\parallel z)\right.\right.$$
$$- \left.\left(J_1^2 + J_0J_2\right)\right] P_\parallel^2\cos(2\varphi)$$
$$+ \left(-J_0^2 - J_2^2P_\parallel^4 + 2J_1^2P_\parallel^2\right)\cos(2k_\parallel z)$$
$$- \left.\left(J_0^2 + J_2^2P_\parallel^4 + 2J_1^2P_\parallel^2\right)\right\} . \quad (36)$$

The radial and azimuthal forces acting on the same object placed in single or standing BB have the same order of magnitude but the axial forces differ significantly. For simplicity let us compare them in the paraxial case $P_\parallel^2 \simeq 0$:

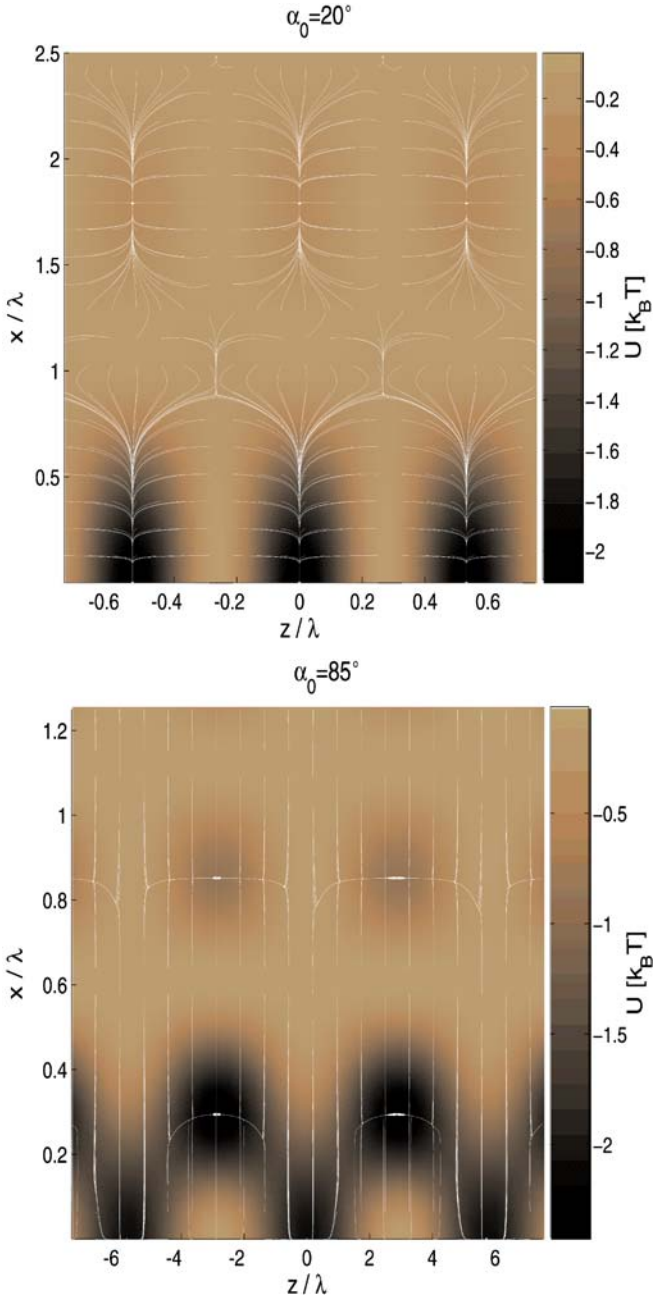

FIGURE 4 z-x potential energy profile of a polystyrene beam placed in two identical counter-propagating Bessel beams. The parameters and symbols were the same as in Fig. 3

$$\max\left(\frac{F_z^{SW}}{F_z}\right) = \max\left(\frac{\alpha'}{\alpha''}\sin(2k_\parallel z)\right) \simeq \frac{3}{2}\frac{m^2+2}{m^2-1}(ka)^{-3} . \quad (37)$$

With respect to (21), the axial force in the standing wave is by several orders of magnitude stronger when comparing to the single BB and moreover, it is modulated by $\sin(2k_\parallel z)$ which gives an array of axial equilibrium positions. Due to the dependencies of $k_\parallel$ and $k_\perp$ on the polar angle α_0, the bigger α_0, the narrower the radial dimension of the trap, but the wider axial extent of the trap (see Fig. 4). For the paraxial beam we got the trap half-width equal to 1.1λ radially and 0.27λ axially. In the case of a non-paraxial beam we get a sub-wavelength radial intensity maximum (its half-width $\simeq 0.38\lambda$) but the distance between neighboring on-axial standing wave maxima is in units of wavelength ($\simeq 2.9\lambda$). Therefore the shorter the trapping wavelength used, the smaller the dimensions of the traps. With increasing strength of the trapping field the objects are better localized close to the trap bottom and so they can be confined in the nanoregion.

Let us compare the axial forces calculated by this Rayleigh approximation with a more exact Mie approach [23]. Figure 5 shows how the size of the object influences the deviation of the Rayleigh approach from the Mie value for a single Bessel beam and a standing Bessel beam. The beam parameters used for calculations coincide with the experimental ones mentioned below. The results reveal that the Rayleigh approach gives a higher value of the axial force and of course completely ignores the sign change of the axial force in the standing wave [23]. Even though the Rayleigh approximation gives axial force values four times bigger when comparing to the Mie value, it can be efficiently used to estimate the trends of the forces acting on the spheres of radius up to 100 nm under the considered conditions.

4 Experimental set-up

We studied experimentally, the confinement of polystyrene particles in an array of optical traps generated by the interference of counter-propagating BBs. In contrast to the previous experiment [17], we used a two times shorter wavelength and identical optical components in both arms (see Fig. 6). Both created BBs had a radius of the intensity

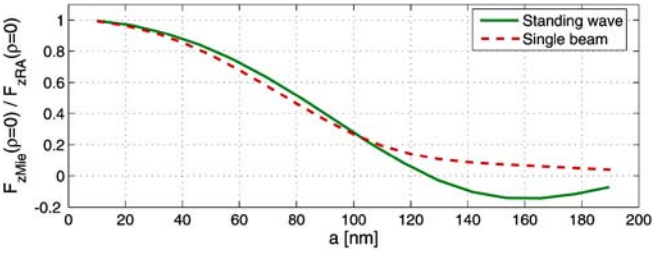

FIGURE 5 Ratio of the axial forces calculated by the Mie approach $F_{z\mathrm{Mie}}$ [23], and the Rayleigh approximation $F_{z\mathrm{RA}}$ for a sphere placed at the centre of a single BB (*dashed curve*) or a standing BB (*full curve*). In the case of the standing wave the maximal (minimal) values of the force along the z-axis are taken if the sphere equilibrium position is placed at the standing wave antinode (node). The radius of the Bessel beam core coincides with the experimental set-up (see below) and the rest of the parameters were the same as in Fig. 3

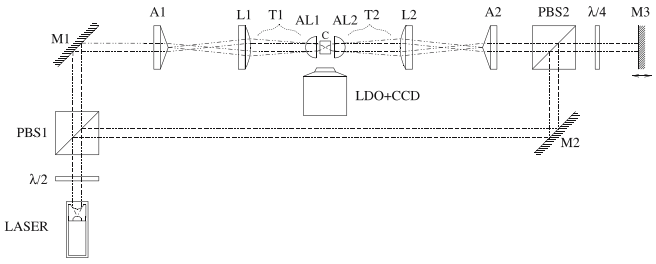

FIGURE 6 The experimental setup with two counter-propagating BBs. Polarisation of the beam from the laser (Coherent Verdi V5, 5 W, $\lambda = 532$ nm) is tuned by the half-wave plate $\lambda/2$ to control the power ratio of beams separated on the polarizing beam-splitter PBS1. The first beam coming through PBS1 is reflected by the dielectric mirror M1 to the axicon A1 (EKSMA 170°), where it is transformed into a BB. Its width is consequently decreased on a telescope T1 consisting from the doublet lens L1 ($f = 30$ mm) and aspherical lens AL1 ($f = 8$ mm). The mirror M2 reflects the second beam towards the polarizing beam-splitter PBS2 which reflects the beam through the quarter-wave plate $\lambda/4$ to the movable mirror M3. Here the beam is reflected backwards through the $\lambda/4$ and PBS2 to the axicon A2 and telescope T2. The optical elements in both parts are the same and so both counter-propagating BBs have the same properties. By the use of movable mirror M3 the phase of the second beam can be tuned in a cuvette C. This causes the movement of the whole structure of standing wave nodes and antinodes together with confined objects. Trapped objects can be recorded by the imaging system consisting of microscope objective LDO and a CCD camera

centre core equal to 1.21 μm. The maximum nondiffracting distance of each beam we define as the distance where the on-axial intensity of the BB beam is higher than $\exp(-1)$ of the on-axial BB intensity maximum. We obtained the maximum nondiffracting distance of about 5 mm in water for each BB for our configuration [31]. Interference of both counter-propagating overlapped beams generated nanotraps separated by 201.6 nm, and arranged into a linear array. Experimentally we observed that this array was filled along the distance of 1 mm with polystyrene beads of radius 175 μm (see Fig. 7). A combination of precise beam alignment and available laser power has not allowed generation of longer array of confined particles. Unfortunately, at the moment we do not fully understand the phenomenon of the dark places in the particle chain. The diffraction on the axicon edges was negligible and we do not see any reason for the axial intensity modulation on this scale coming from the beam. We speculate that it could be caused by the collective scattering of many confined particles.

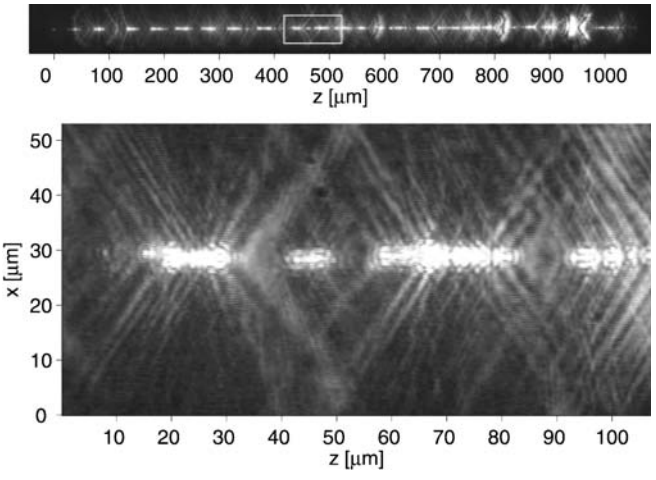

FIGURE 7 1 mm long array of polystyrene particles of 175 nm in radius captured in the Bessel beam generated standing wave. The *top image* is composed from 10 frames taken at different positions of the imaging system (LDO + CCD). The *bottom image* shows part of one unscaled frame corresponding to the *white rectangle* from the top image

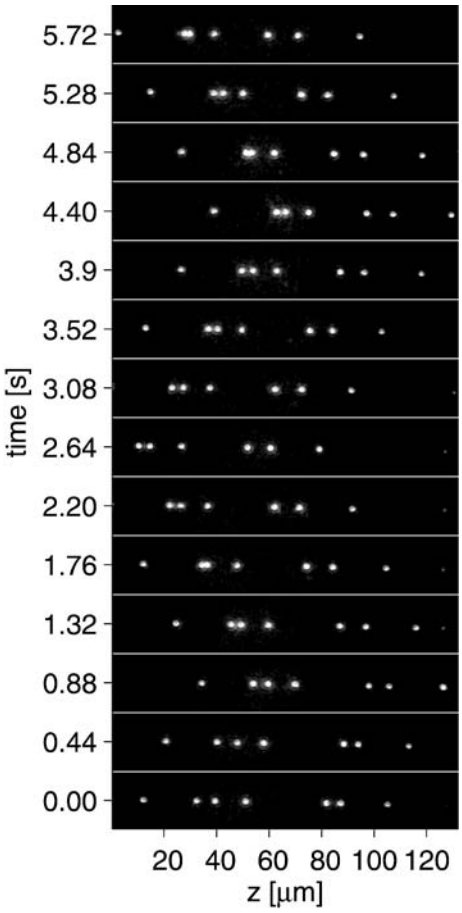

FIGURE 8 Simultaneous confinement and delivery of polystyrene particles of radius 100 nm in a movable standing Bessel wave (optical conveyor belt)

Since the movable mirror M3 changes the phase in one beam, the whole structure of intensity maxima and minima moves axially, followed by the confined objects. Figure 8 proves the delivery of polystyrene beads of radius 100 nm over a distance of 60 μm. Since both BBs axially overlapped over a distance exceeding 1 mm, the same mechanism was used to deliver the objects over 1 mm.

5 Conclusions

We presented a non-paraxial description of the ideal Bessel beam created behind the axicon illuminated by a linearly polarized beam. Using this description we described the optical force acting on nanoparticles placed into such a beam, and the standing wave made of two such beams. Based on this knowledge and previous experiments we succeeded in optical confinement of small objects such as polystyrene beads of radius 100 nm dispersed in water. They formed a one-dimensional 1 mm long array. On changing the phase of one beam we were able to move these objects over 1 mm.

ACKNOWLEDGEMENTS The authors thank Prof. Z. Bouchal, Prof. K. Dholakia, and Dr. V. Garcés-Chávez for stimulating comments and discussion. This work was partially supported by the EC 6FP NEST ADVENTURE Activity (ATOM3D, project No. 508952), ISI IRP (AV0Z20650511), and MCT (FT-TA2/059).

REFERENCES

1 L. Polonskiy, Sov. J. Quantum Electron. **16**, 178 (1986)
2 J. Durnin, J.J. Miceli, J. Eberly, Phys. Rev. Lett. **58**, 1449 (1987)
3 Z. Bouchal, J. Wagner, M. Chlup, Opt. Commun. **151**, 207 (1998)
4 M.R. Lapointe, Opt. Laser Technol. **24**, 315 (1992)
5 J.H. McLeod, J. Opt. Soc. Am. **44**, 592 (1954)
6 V. Garcés-Chávez, D. McGloin, H. Melville, W. Sibbett, K. Dholakia, Nature **419**, 145 (2002)
7 D. McGloin, K. Dholakia, Contemp. Phys. **46**, 15 (2005)
8 B.P.S. Ahluwalia, X.C. Yuan, S.H. Tao, J. Bu, H. Wang, X. Peng, H.B. Niu, Appl. Phys. Lett. **87**, 084 104 (2005)
9 V. Garcés-Chávez, D. Roskey, M.D. Summers, H. Melville, D. McGloin, E.M. Wright, K. Dholakia, Appl. Phys. Lett. **8**, 4001 (200)
10 P. Fischer, C.T.A. Brown, J.E. Morris, C. López-Mariscal, E.M. Wright, W. Sibbett, K. Dholakia, Opt. Express **13**, 6657 (2005)
11 M. Rioux, R. Tremblay, P.A. Belanger, Appl. Opt. **17**, 1532 (1978)
12 J.A. Davis, E. Carcole, D.M. Cottrell, Appl. Opt. **35**, 2159 (1996)
13 Z. Ding, H. Ren, Y. Zhao, J.S. Nelson, Z. Chen, Opt. Lett. **27**, 243 (2002)
14 J. Arlt, K. Dholakia, J. Soneson, E.M. Wright, Phys. Rev. A **63**, 063 602 (2001)
15 D. McGloin, V. Garcés-Gávez, K. Dholakia, Opt. Lett. **28**, 657 (2003)
16 T. Čižmár, V. Garcés-Chávez, K. Dholakia, P. Zemánek, In: *Optical Trapping and Optical Micromanipulation: Proc. of SPIE*, ed. by K. Dholakia, G.C. Spalding, **5514**, 643 (2004)
17 T. Čižmár, V. Garcés-Chávez, K. Dholakia, P. Zemánek, Appl. Phys. Lett. **86**, 174 101 (2005)
18 Z. Bouchal, R. Horák, J. Wagner, J. Mod. Opt. **43**, 1905 (1996)
19 Z. Bouchal, J. Kyvalský, J. Mod. Opt. **51**, 157 (2004)
20 S. Chávez-Cerda, M.A. Meneses-Nava, J.M. Hickmann, Opt. Lett. **23**, 1871 (1998)
21 T. Saastamoinen, J. Tervo, P. Vahimaa, J. Turunen, J. Opt. Soc. Am. A **21**, 1424 (2004)
22 B.P.S. Ahluwalia, X.C. Yuan, S.H. Tao, Opt. Commun. **238**, 177 (2004)
23 T. Čižmár, V. Kollárová, Z. Bouchal, P. Zemánek, New J. Phys. **8**, 43 (2006)
24 Z. Bouchal, M. Olivík, J. Mod. Opt. **42**, 1555 (1995)
25 Y. Zhang, L. Wang, C. Zheng, J. Opt. Soc. Am. A **22**, 2542 (2005)
26 J.J. Stamnes, *Waves in Focal Regions* (IOP, Bristol, 1986)
27 J. Fagerholm, A.T. Friberg, J.H. Huttunen, D.P. Morgan, M.M. Salomaa, Phys. Rev. E **54**, 4347 (1996)
28 P. Chaumet, M. Nieto-Vesperinas, Opt. Lett. **25**, 1065 (2000)
29 B. Draine, Astrophys. J. **333**, 848 (1988)
30 P. Zemánek, A. Jonáš, L. Šrámek, M. Liška, Opt. Lett. **24**, 1448 (1999)
31 V. Jarutis, R. Paškaustas, A. Stabinis, Opt. Commun. **184**, 105 (2000)